Insights and emerging directions from Force-Balance based Joint Inversion of GNSS and InSAR

Mradula Vashishtha [1], William Holt[1], Jeonghyeop Kim[2]

1 Stony Brook University
2 Kangwaon National University

Correspondence: mradula.vashishtha@stonybrook.edu

Acknowledgments:
This research has been sponsored by SCEC grant **24177, 25322** and NASA [**FINESST program 80NSSC19K1367; ESI 80NSS-C21K0838**

Highlights

- Southern California exhibits complex deformation patterns and fault systems.
- We combine the strengths of GNSS and InSAR using the joint inversion to overcome their spatial and directional limitations respectively.
- We employ a physics-based approach based on solutions of the force balance equations on a sphere using the weak formulation in finite elements.
- We obtain basis function responses to force rate couples $\emptyset\emptyset$, $\emptyset\theta$ and $\theta\theta$ in the horizontal and for Ur/r for the vertical basis function response. For the spherical case the vertical response is weakly coupled to the horizontal.
- Solutions can also be expressed in terms of the input force rate couples, which are the vertical derivative of horizontal shear stress (VDoHS) rate $\frac{\partial \sigma_{r\phi}}{\partial z}$ and $\frac{\partial \sigma_{r\theta}}{\partial z}$.
- We use this joint inversion algorithm to provide an estimate of a time-averaged strain rate field (15-year average), rotation rates, and vertical gradients of horizontal shear stress (VDoHS) rates.
- We also develop a method to determine the velocity field and full strain rate tensor at depth within the crust.
- We investigate the gradients of force rates (divergence and shear), eigenvectors of these gradient fields, and directions of zero change in these gradient fields.
- We show these gradient fields yield insights into the dynamics of the elastic field including fault locking depths, slip rates, maximum shear orientations and their locations.
- The Force-Balance approach yields insights into the source of off-fault deformation. Along strike slip rate changes typically result in basin formation in areas containing the major strike slip faults and adjacent shortening in directions nearly perpendicular to the strike of transform faults

Force Balance

$$\frac{\partial \sigma_{rx}}{\partial r} + \frac{\partial \sigma_{xy}}{\partial y} + \frac{\partial \sigma_{xz}}{\partial z} = 0$$
$$\frac{\partial \sigma_{ry}}{\partial r} + \frac{\partial \sigma_{xy}}{\partial y} + \frac{\partial \sigma_{yz}}{\partial z} = 0$$
$$\frac{\partial \sigma_{rz}}{\partial r} + \frac{\partial \sigma_{yz}}{\partial y} + \frac{\partial \sigma_{zz}}{\partial z} + \frac{\partial (\rho g \delta)}{\partial t} = 0$$

where σ_{ij} is the stress rate

Solution to the force balance equations is obtained by minimizing the J functional :

$$J = \iint \{[(\dot{\bar{\varepsilon}}) - (\bar{\Phi}_i)]^T V^{-1} [(\dot{\bar{\varepsilon}}) - (\bar{\Phi}_i)]\} \cos\theta d\emptyset d\theta$$

where ε is the strain rate, V^{-1} is equivalent to the elasticity tensor and $\bar{\Phi}_i$ is the vector potential. $\bar{\Phi}_1 = (\Phi_{\phi\phi} \ 0 \ 0)^T$, $\bar{\Phi}_2 = (0 \ \Phi_{\theta\theta} \ 0)^T$, $\bar{\Phi}_3 = (0 \ 0 \ \Phi_{\phi\theta})^T$ and $\bar{\Phi}_4 = \left(\frac{u_r}{r} \ \frac{u_r}{r} \ 0\right)^T$

$$f_\emptyset = -\frac{1}{r\cos\theta}\frac{\partial}{\partial \emptyset}(\mu\varepsilon_{\emptyset\emptyset} - \mu\varepsilon_{\theta\theta}) + \frac{1}{r} 4\mu\varepsilon_{\emptyset\theta} tan\theta - \frac{\partial}{r\partial\theta}(2\mu\varepsilon_{\emptyset\theta}) - \frac{1}{r\cos\theta}\frac{\partial}{\partial\emptyset}\{(3\mu(\varepsilon_{\emptyset\emptyset}+\varepsilon_{\theta\theta})\}$$

$$f_\theta = \frac{\partial}{r\partial\theta}(\mu\varepsilon_{\emptyset\emptyset} - \mu\varepsilon_{\theta\theta}) - \frac{2}{r}(\mu\varepsilon_{\emptyset\emptyset} - \mu\varepsilon_{\theta\theta}) tan\theta - \frac{1}{r\cos\theta}\frac{\partial}{\partial\emptyset}(2\mu\varepsilon_{\emptyset\theta}) - \frac{\partial}{r\partial\theta}\{(3\mu(\varepsilon_{\emptyset\emptyset}+\varepsilon_{\theta\theta})\}$$

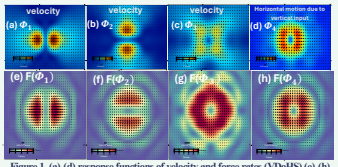

Figure 1. (a)-(d) response functions of velocity and force rates (VDoHS) (e)-(h) in response to input potentials $\bar{\Phi}_i$.

Joint Inversion

$$\begin{bmatrix} \boldsymbol{d}_{GNSS} \\ \boldsymbol{d}_{InSAR} \\ in\ ITRF14\ frame \end{bmatrix} = \begin{bmatrix} G \\ body\ force\ equivalent\ input \\ of \Phi_1, \Phi_2, \Phi_3, \Phi_4 \end{bmatrix} [\boldsymbol{m}]$$

$$u_{InSAR} = \hat{p} \cdot [(W(\hat{r}) \times r) + u_r(\hat{r})], u_{GNSS} = (W(\hat{r}) \times r)$$

$W(\hat{r})$ is the vector rotation function on the surface of a sphere, $\hat{p}$ is the unit pointing vector from ground to satellite and u_r is is the velocity in the radial direction of the Earth on the surface.

The best-fit linear combination of response functions that can predict GNSS and InSAR is obtained by performing **Ridge regularization (L2 norm).**

Steady-state deformation can be expressed as:

$$\underset{total\ deformation}{\boldsymbol{u}} = \underset{boundary\ motion}{\boldsymbol{u}} + \underset{internal\ deformation}{\boldsymbol{u}}$$

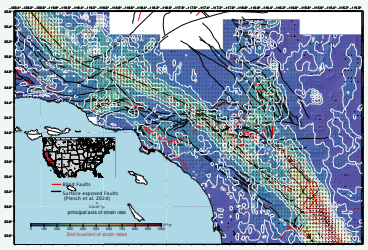

Figure 2 . Estimated Horizontal strain rate field from the Joint Inversion.

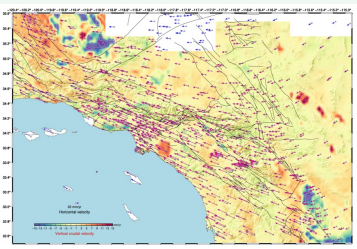

Figure 3. Input GNSS velocities from Blewitt et al. 2016 (NGL's MIDAS) and Zeng 2022 in blue arrows and predicted velocities from the Joint Inversion in voilet arrows. Horizontal velocities are in an ITRF14.

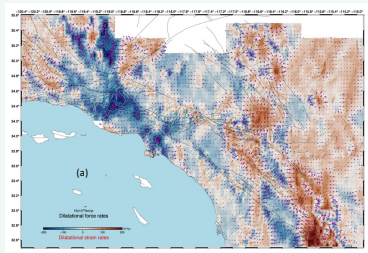

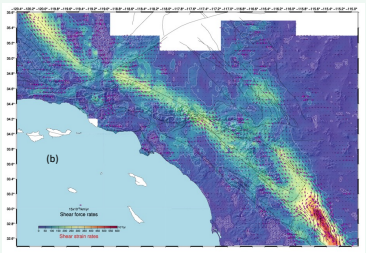

Figure 4. (a) Dilatational and (b) Shear component of force rates (Vertical derivative of horizontal shear stress rates VDoHS) at the surface obtained from the Joint Inversion.

Implications for along-strike slip-rate variation in force rate field

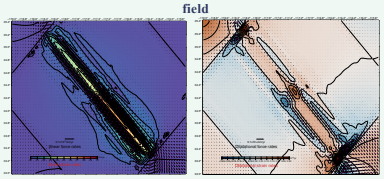

Figure 5.

1-dimensional functional forms of horizontal component surface velocities, strain rates, VDoHS rates and gradients of force rates for a vertical strike-slip fault

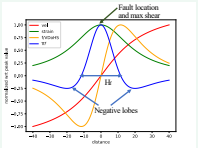

Figure 6. Hr is the peak width for gradient of force rates, bounded by double lobes of opposite sign. Fault locking depth is 0.87Hr.

Strain rates and velocities with depth :

Assume linear relationship of gradients of velocity with depth:

$$\frac{\partial u_x}{\partial x}(z) = a_1 z + b_1$$
$$\frac{\partial u_x}{\partial y}(z) = a_2 z + b_2$$
$$\frac{\partial u_x}{\partial z}(z) = a_3 z + b_3$$
$$\frac{\partial u_y}{\partial z}(z) = a_4 z + b_4$$

At z=0, $\frac{\partial u_x}{\partial x} = \frac{\partial u_x}{\partial x}$ and $\frac{\partial u_x}{\partial y} = \frac{\partial u_x}{\partial y}$ gives b coefficients.

Assuming $\frac{\partial \omega_{xz}}{\partial z} = 0$ gives a coefficients.

$$u_x(z) = \frac{\partial \varepsilon_{xz}}{\partial z}\frac{z^2}{2} + \left(-\frac{\partial u_z(0)}{\partial x}\right) z + u_x(0) \quad (1)$$

$$u_y(z) = \frac{\partial \varepsilon_{yz}}{\partial z}\frac{z^2}{2} + \left(-\frac{\partial u_z(0)}{\partial y}\right) z + u_y(0) \quad (2)$$

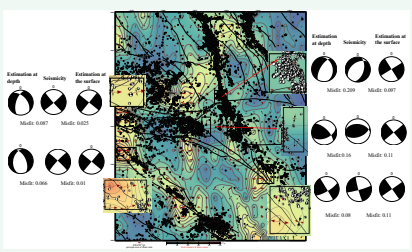

Figure 10. Comparison of strain tensor with the Kostrov summed moment tensors (Cheng et al. 2021) for both surface and at depth (10 km).

Figure 11. Mid crustal dilatation inferred from extrapolation of surface VDoHS using equations (1) and (2).

Implications for Patterns of Mid - Lower Crustal Flow

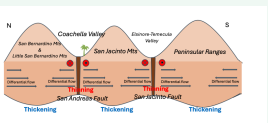

Spatial gradients of force rate and implication for fault related deformation field

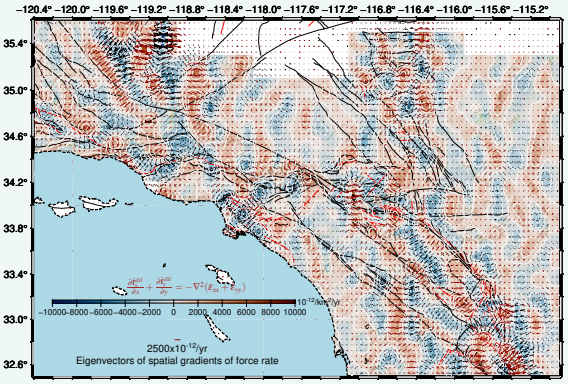

Figure 7. Contoured background shows divergence of spatial gradients of dilatational component of force rate field. Eigenvectors of spatial gradients of force rates, equal to directions of maximum (convergence rate) and minimum (divergence rate) in force rate gradients.

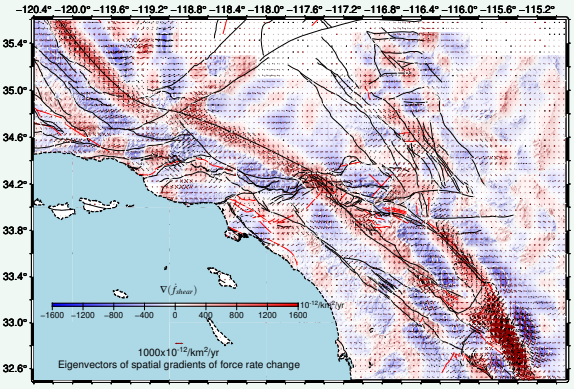

Figure 8. Background shows the shear component of the spatial gradient field of force rates G1_F = (dFx/dx – dFy/dy). The arrows show eigenvectors of spatial gradient of force rate change, as in Figure 7. The width of the belt of positive G1_F (labeled Hr in Figure 6) that runs parallel to the major strike-slip transform faults is proportional to fault locking depth. Note that double lobes of opposite sign, on either side of the positive anomaly, is a signature of elastic locking on major transform faults.

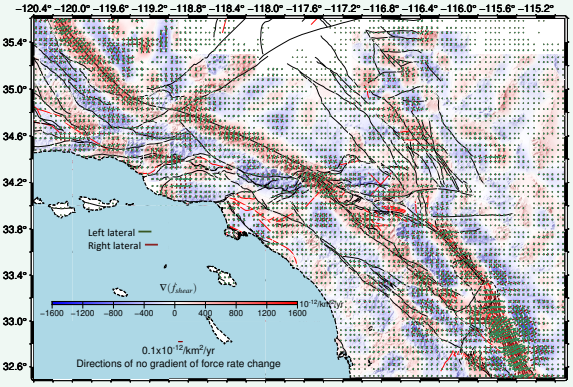

Figure 9. Background shows the shear component of the spatial gradient field of force rates G1_F = (dFx/dx – dFy/dy). The bars show directions along which the spatial gradients in force rate are zero. These directions align with major strike-slip structures and their magnitudes (length of lines) also predict location of maximum shear along with the sense of slip (right-lateral or left-lateral) on those faults.

References

Blewitt, Geoffrey, Corné Kreemer, William C. Hammond, and Julien Gazeaux. 2016. "MIDAS Robust Trend Estimator for Accurate GPS Station Velocities without Step Detection." *Journal of Geophysical Research: Solid Earth* 121 (3): 2054–68. https://doi.org/10.1002/2015JB012552.

Cheng, Yifang, Egill Hauksson, and Yehuda Ben-Zion. 2023. "Refined Earthquake Focal Mechanism Catalog for Southern California Derived With Deep Learning Algorithms." *Journal of Geophysical Research: Solid Earth* 128 (2): e2022JB025975. https://doi.org/10.1029/2022JB025975.

Ghosh, A., Holt, W. E., & Flesch, L. M. (2009). Contribution of gravitational potential energy differences to the global stress field. *Geophysical Journal International*, *179*(2), 787-812.

Plesch, A., Marshall, S. T., Shaw, J. H., Su, M., Maechling, P. J., Huynh, T. T., & Funk, S. (2024, 09). CFM 7.0: Integration of southern, central, and northern California 3d fault representations into a uniform, statewide Community Fault Model. Poster Presentation at 2024 SCEC Annual Meeting.

Zeng, Yuehua. 2022. "GPS Velocity Field of the Western United States for the 2023 National Seismic Hazard Model Update." *Seismological Research Letters* 93 (6): 3121–34. https://doi.org/10.1785/0220220103.